Schedae Informaticae Vol. 21 (2012): 81–105
doi: 10.4467/20838476SI.12.006.0816

Optimal Control of a Drying Process with Avoiding Cracks

Alexander Galant[2], Christian Grossmann[1],
Michael Scheffler[2], Jörg Wensch[1]

[1]Fachrichtung Mathematik, [2]Fakultät Maschinenwesen,
Technische Universität Dresden
01062 Dresden, Germany

Abstract. The paper deals with the numerical treatment of the optimal control of drying of materials which may lead to cracks. The drying process is controlled by temperature, velocity and humidity of the surrounding air. The state equations define the humidity and temperature distribution within a simplified wood specimen for given controls. The elasticity equation describes the internal stresses under humidity and temperature changes. To avoid cracks these internal stresses have to be limited. The related constraints are treated by smoothed exact barrier-penalty techniques. The objective functional of the optimal control problem is of tracking type. Further it contains a quadratic regularization by an energy term for the control variables (surrounding air) and barrier-penalty terms.

The necessary optimality conditions of the auxiliary problem form a coupled system of nonlinear equations in appropriate function spaces. This optimality system is given by the state equations and the related adjoint equations, but also by an approximate projection onto the admissible set of controls by means of barrier-penalty terms. This system is discretized by finite elements and treated iteratively for given controls. The optimal control itself is performed by quasi-Newton techniques.

2000 AMS subject classifications: 90C25, 90C51, 49K20, 65K10

Keywords: optimal control, penalty barrier methods, control constraints, coupled parabolic system, discretization.

1. Introduction

The considered models lead to systems of two parabolic partial differential equations in three spatial variables. This pde system incorporates also phase changes which e.g. occur in the coupling terms of the system. Diffusion coefficients depend in a complex way on the state of the system and these dependencies have to be estimated by experiment. The same holds for the parameters of the evolution equations which describe phase changes. In our model the relevant state variables are temperature and moisture content of the material. Thus, we obtain an optimal control problem with a coupled system of time dependent initial-boundary value problems as state equations (cf. [24]). The numerical solution of the direct problem requires discretization in time and space. Time discretization is done by the implicit Euler method. The resulting elliptic system is discretized by the conforming Finite Element method on a triangular grid with linear elements. The drying process is controlled via the boundary values, namely temperature, moisture and velocity of the surrounding air. The objective of the process is to reduce the moisture of wood up to a prescribed degree under minimal energy. In order to avoid cracks (see [20]), restrictions on internal tensions are treated by a smoothed exact penalty method (see [11]). An efficient evaluation of gradients via the adjoint system for the time-discretized model is applied.

As a particular example we consider the industrial wood drying performed in drying chambers. On the one hand, a simplified form of this technological process fits directly into the discussed general approach and on the other hand some functional dependencies from wood drying are used to illustrate the model. The wood drying process is controlled by various functions like outer temperature, humidity and velocity of the surrounding air. The aim of the present paper is to report on an optimization approach to this task by gradient based methods. In the literature there is a rather wide variety of models for wood drying, see e.g. [4, 5, 12, 14, 19, 25, 16].

Models based on physical principles use a multiple component approach. There are three phases of water, namely liquid water, vapor and bound water. Phase changes occur due to pressure and temperature variations. Fluid transport is caused mainly by diffusion. In addition, advection may be caused by pressure gradients. Vapor is modeled as a component of a mixture of air and vapor underlying advection and diffusion. Advection and diffusion of vapor is computed as multi component flow of the air-vapor mixture driven by pressure and concentration gradients.

The drying process is controlled via the boundary values, namely temperature, moisture and velocity of the surrounding air. The objective of the process is to reduce the moisture of wood up to a prescribed degree under minimal energy. In order to avoid cracks (see [20]), restrictions on internal tensions are included into the problem by a smoothed exact penalty method (see [11]). For results on optimal control of partial differential equations, we refer e.g. to [3, 11, 13, 24]. Having gradient based optimization as optimization technique in mind the efficient evaluation of gradients via adjoint systems is studied in Section 3. In particular, the adjoint system for the time-discretized model is derived.

The paper is structured as follows. In Section 2 we describe a rather abstract

formulation of the underlying model for the direct problem as a system of evolution equations. Further the discretization by finite elements is briefly described and the gradient evaluation via adjoints is outlined. A simplified model of wood drying is derived in Section 3. In Section 4 we report on numerical results, both, the direct simulation with discretization techniques as well as the solution of the optimal control problem by gradient-based techniques of Quasi-Newton type. Finally a short summary in Section 5 concludes the paper.

2. The abstract control problem

2.1. The control problem

In this section we discuss a class of boundary optimal control problems with a system of quasi-linear parabolic partial differential equations as state equations and pointwise control and nonlinear state constraints. Many application problems can be embedded into this general framework.

We consider the nonlinear control problem

$$J(y,u) := \sum_{i=1}^{n} \frac{\mu_i}{2} \int_\Omega (y_i(\cdot,T) - y_{d,i})^2 \, d\Omega + \sum_{j=1}^{m} \frac{\alpha_j}{2} \int_0^T (u_j - u_{d,j})^2 \, dt \longrightarrow \min \quad \text{(1a)}$$

subject to

$$\begin{array}{rcll} y_t + \mathscr{A}(y)y &=& 0, & \text{in } \Omega \times (0,T] \\ \mathscr{B}(y)y &=& g(y,u), & \text{on } \Gamma \times (0,T] \\ y(\cdot,0) &=& y^0 & \text{on } \overline{\Omega} \end{array} \quad \text{(1b)}$$

$$\begin{array}{rcl} u_a \leq & u & \leq u_b \\ \sigma_a \leq & \sigma(y) & \leq \sigma_b. \end{array} \quad \text{(1c)}$$

In this setting $\Omega \subset \mathbb{R}^N, N \in \mathbb{N}$ denotes a bounded domain which has a piecewise $C^{1,1}$ boundary Γ and T is a fixed time horizon. For a given initial value y^0 we will seek the optimal control $u : [0,T] \to \mathbb{R}^m$ with associated optimal state $y : \Omega \times [0,T] \to \mathbb{R}^n$. The objective functional J represents a classic form, in which the first term is of tracking type that minimizes the difference between the state values $y(\cdot,T)$ at the end time T and the target values y_d. The second term is a regularization, where u_d denotes some energy minimal control. The parameters μ_i and α_j are scaling and regularization parameters, respectively. We consider bounds $u_a, u_b \in \mathbb{R}^m, u_a \leq u_b$ and $\sigma_a, \sigma_b \in \mathbb{R}, \sigma_a \leq \sigma_b$. The operator $\mathscr{A}(y)$ is (uniformly) elliptic of the type

$$\mathscr{A}(y)z = -\sum_{j,k}^{N} \partial_j (a_{jk}(y) \partial_k z) \quad \text{(2)}$$

and $\mathscr{B}(y)$ denotes the related boundary operator of Neumann type. Moreover, the nonlinear functions $\sigma : \mathbb{R}^n \to \mathbb{R}$, $\quad g : \mathbb{R}^n \times \mathbb{R}^m \to \mathbb{R}^n$ and $a_{jk} : \mathbb{R}^n \to \mathbb{R}^{n\times n}$, $j, k = 1, \ldots, N$ are given.

In the sequel we apply the following notation: By $(\cdot, \cdot)$ and $\|\cdot\|$ we denote the inner product in $L_2(\Omega)$ and the related norm, respectively. Further, we introduce following spaces with usual product topologies $\mathbf{V} := H^1(\Omega)^n$, $\mathbf{H} := L_2(\Omega)^n$ and $\mathbf{U} := L_\infty(0,T)^m$. With $< \cdot, \cdot >$ we denote duality pairing between $\mathbf{V}$ its dual space $\mathbf{V}^*$.

Let us start the discussion with the state equations (1). The abstract problem (1b) can be described by a system of variational equations. With the bilinear form

$$a(y; \cdot, \cdot) : \mathbf{V} \times \mathbf{V} \to \mathbb{R} \qquad \text{defined by} \qquad a(y; z, v) := \sum_{j,k=1}^{N} \int_\Omega a_{jk}(y) \partial_k z \cdot \partial_j v \, d\Omega$$

and the linear form

$$(g(y,u), \cdot)_\Gamma : \mathbf{V} \to \mathbb{R}$$

defined by

$$(g(y,u), v)_\Gamma := \int_\Gamma g(y,u) \cdot v \, d\Gamma \quad \text{for all} \quad (y,u) \in \mathbf{V} \times \mathbf{U},$$

we obtain the following weak formulation:

$$\begin{aligned} \langle y_t, v\rangle + a(y; y, v) = &\quad (g(y,u), v)_\Gamma \qquad \forall\, v \in \mathbf{V} \quad t \in (0,T], \\ y(0) = &\quad y^0. \end{aligned} \tag{3}$$

For our further analysis we introduce the set of admissible controls for (1) by

$$U_{ad} := \{u \in U : \; u_a \le u(\cdot) \le u_b \quad \text{a.e. in } (0,T)\}.$$

Theorem 1. *Under the assumptions:*

A1: Ω be a bounded region in $\mathbb{R}^N$ with $\partial\Omega \in C^\infty$;

A2: The coefficients g, $a_{jk}, \forall j, k = 1, \ldots, N$ are C^∞ for all $y \in \overline{\Omega}$ and $u \in \overline{U}_{ad}$;

A3: (Ellipticity of $\mathscr{A}$): for each $y \in \mathbb{R}^n$ and $\xi \in \mathbb{R}^n$ with $|\xi| = 1$, all the eigenvalues of the $n \times n$-matrix $a_{jk}(y)\xi_j\xi_k$ have a positive real part;

the following statements are true:

(a) (Existence and Uniqueness): For any $(y^0, u) \in \mathbf{H} \times \mathbf{U}$ the parabolic initial-boundary value problem (1b) *possesses a unique (weak) solution $y \in W(0,T)$, where the space $W(0,T)$ is given by $W(0,T) := \{\, y \in L_2(0,T,\mathbf{V}) : \; y_t \in L_2(0,T,\mathbf{V}^*)\,\}$.*

(b) (Differentiability): The solution $y(t)$ depends in the topology of $W(0,T)$ smoothly upon y^0 and u. Particularly, for each $w \in \mathbf{U}$ the function

$$p(\cdot) = \partial_u y(\cdot, y^0, u) w$$

is equal to the solution of the initial-boundary value problem, which is obtained by differentiating the original problem (1b) *formally with respect to u in the directional w.*

For the proof we refer to [1] Theorem 7.1, 7.3 and 11.1 as well as to [27] Theorem 31.C.

Hence, by Theorem 1, the parabolic initial-boundary value problem governing (1) admits for each $u \in U_{ad}$ a unique weak solution $y \in W(0,T)$. This allows us to introduce the control-to-state operator $S : U_{ad} \to W(0,T) : u \mapsto y$. With this setting we will reformulate the general problem to the reduced form:

$$f(u) := J(S(u), u) \longrightarrow \min! \tag{4a}$$

subject to

$$u \in U_{ad}, \qquad \sigma_a \leq \sigma(S(u)) \leq \sigma_b. \tag{4b}$$

For the treatment of the state constraint (4b) we apply the penalization technique, based on smoothed exact penalty function

$$\eta \left(a - \xi + \sqrt{(a-\xi)^2 + s^2} \right)$$

with the parameters η, $s \in \mathbb{R}$ which for $s \to 0+$ approximates the well known exact penalty

$$2\,\eta \max\{0, a - \xi\}$$

to treat the constraint $a - \xi \leq 0$. In the considered case of (4b) this leads up to a constant to

$$\begin{aligned} P_\eta(\xi; a, b, s) &:= \eta \left(\sqrt{(\xi - a)^2 + s^2} + \sqrt{(\xi - b)^2 + s^2} \right) \\ &\approx \eta \left(|\xi - a| + |\xi - b| \right), \end{aligned} \tag{5}$$

where $s > 0$ is a smoothing parameter that tends in the limit to 0, and $\eta > 0$ is a fixed parameter that is sufficiently large to ensure the exactness of underlined penalty $\eta\,(|\xi - a| + |\xi - b|)$ (cf. [10]). We, hence, consider a purely control-constrained and smooth problem

$$f_\eta(u) := f(u) + \int_0^T \int_\Omega P_\eta(\sigma(S(u)); \sigma_a, \sigma_b, s)\, d\Omega\, dt \longrightarrow \min_{u \in U_{ad}}, \tag{6}$$

where the state constraints have been handled by penalization (5). For the convergence of this barrier-penalty method in the finite dimensional case we refer to [10]. We meet this case later since the problem will be discretized by finite elements.

We remark that in the case of the infinite problem the constraints upon $\sigma(y)$ have to be considered pointwise to guarantee the existence of optimal Lagrange multipliers, which in this case are Borel measures.

Under certain additional conditions, e.g. linearity of the control in the state equation, one can show the existence of at least one globally optimal control u^* with associated optimal state y^* for (6), provided the set of admissible controls U_{ad} is not empty. The associated first-order necessary optimality conditions can be determined by a standard computation.

Theorem 2. *Let $u^* \in U_{ad}$ be a solution of (6) with the associated optimal state y^*. Under the assumption*

A4: The function σ is bounded and continuously differentiable with $\partial_y \sigma(y^*) \in V^*$ for $t \in (0,T]$.

we have:

(a) The adjoint variational equation

$$\begin{aligned} \langle \lambda_t, v\rangle + \quad & a(y^*; v, \lambda) + a_y(y^*; v, \lambda) - (\partial_y g(y^*, u^*)v, \lambda)_\Gamma \\ = \quad & \int_\Omega P'_\eta(\sigma(y^*); \sigma_a, \sigma_b, s)\langle \partial_y \sigma(y^*),\ v\rangle \, d\Omega \quad \forall\, v \in \mathbf{V}, \quad t \in [0,T) \qquad (7) \\ \lambda_i(T) = \quad & \mu_i(y_i^*(T) - y_{d,i}). \end{aligned}$$

admits for every pair $(y^*, u^*) \in \mathbf{V} \times U_{ad}$ a unique (weak) solution $\lambda^* \in W(0,T)$, where the bilinear form $a_y(y; \cdot, \cdot) : \mathbf{V} \times \mathbf{V} \to \mathbb{R}$ is defined by

$$a_y(y; z, v) := \sum_{j,k=1}^{N} \int_\Omega [\partial_y a_{jk}(y) z] \partial_k y \cdot \partial_j v \, d\Omega.$$

(b) With the adjoint state λ^* the structure of the Frechet derivative of $f_\eta(u^*)$ is given by

$$\langle f'_\eta(u^*), w\rangle = \sum_{j=1}^{m} \alpha_j \int_0^T (u_j^* - u_{d,j}) w_j \, dt + \int_0^T \int_\Omega (\partial_u g(y^*, u^*) w, \lambda^*)_\Gamma \, d\Omega \, dt.$$

(c) The variational inequality

$$\langle f'_\eta(u^*), u - u^*\rangle \geq 0 \quad \forall\, u \in U_{ad}. \qquad (8)$$

is satisfied.

2.2. Discretization

For the numerical treatment of the optimal control problem we have to discretize the objective function (6) and the state equation (3). In order to obtain a complete discretization we use Rothe's method – first discretizing in time, then in space.

Let be selected an equidistant time grid $\{t^k\}_{k=0}^M$ on the time interval $[0,T]$ with grid size $\tau := T/M$. Let y_τ or u_τ denote the (semi-)discrete approximation of $y \in W(0,T)$ or $u \in \mathbf{U}$, defined as piecewise constant function by

$$\begin{aligned} y_\tau(\cdot, t) := \quad & y^k(x) \quad := y(\cdot, t^k) \qquad \forall t \in (t^{k-1}, t^k], \quad k = 1, \ldots, M, \\ u_\tau(t) := \quad & u^k \quad := u(t^k) \qquad \forall t \in (t^{k-1}, t^k], \quad k = 1, \ldots, M. \end{aligned}$$

For the approximation of the time derivative we apply the backward Euler scheme with frozen coefficients in nonlinear terms. This leads to the following semi-discrete

optimal control problem:

$$\begin{aligned} J_\eta^\tau(y_\tau, u_\tau) \quad &:= \quad \textstyle\sum_{i=1}^n \frac{\mu_i}{2} \|y_i^M - y_{d,i}\|^2 + \tau \sum_{j=1}^m \frac{\alpha_j}{2} \sum_{k=1}^M (u_j^k - u_{d,j})^2 \\ &\quad + \tau \textstyle\sum_{k=1}^M \int_\Omega P_\eta(\sigma(y^k); \sigma_a, \sigma_b, s)\, d\Omega \longrightarrow \min \end{aligned} \tag{9a}$$

subject to constraints given by the semi-implicit discretization

$$\frac{1}{\tau}(y^k - y^{k-1}, v) + a(y^{k-1}; y^k, v) = (g(y^{k-1}, u^k), v)_\Gamma, \ \forall\, v \in \mathbf{V}, k = 1, \ldots, M \tag{9b}$$

$$u_\tau \in U_{ad}^\tau, \tag{9c}$$

where y^0 is given by the initial conditions. For the discretization in space we introduce an inner convergent approximation of space $\mathbf{V}$ set by the triples family $(\mathbf{V}_h, p_h, r_h)_{h \in \mathscr{H}}$, where
$\mathbf{V}_h$ – space of linear conform finite elements,
p_h – prolongation operator from $\mathbf{V}_h$ to $\mathbf{V}$ given by identity,
r_h – restriction operator from $\mathbf{V}$ to $\mathbf{V}_h$ defined as L_2-projection.
Further, we define $y_{\tau,h}$ as a finite element approximation of y_τ by

$$y_{\tau,h}(\cdot, t) := y_h^k(\cdot) := r_h y_\tau(\cdot, t) \quad \forall t \in [t^{k-1}, t^k], \quad k = 1, \ldots, M.$$

The full discretization of the control problem is finally obtained from (9) by the use of finite-dimensional space $\mathbf{V}_h$ instead of the space $\mathbf{V}$:

$$\begin{aligned} J_\eta^{\tau,h}(y_{\tau,h}, u_\tau) \quad &:= \quad \textstyle\sum_{i=1}^n \frac{\mu_i}{2} \|y_{h,i}^M - r_h y_{d,i}\|^2 + \tau \sum_{j=1}^m \frac{\alpha_j}{2} \sum_{k=1}^M (u_j^k - u_{d,j})^2 \\ &\quad + \tau \textstyle\sum_{k=1}^M \int_\Omega P_\eta(\sigma(y_h^k); \sigma_a, \sigma_b, s)\, d\Omega \longrightarrow \min \end{aligned} \tag{10a}$$

subject to

$$\begin{aligned} \tfrac{1}{\tau}(y_h^k - y_h^{k-1}, v_h) + a(y_h^{k-1}; y_h^k, v_h) = \quad & (g(y_h^{k-1}, u^k), v_h)_\Gamma \quad \forall\, v_h \in \mathbf{V}_h, k = 1, \ldots, M, \\ y_h^0 = \quad & r_h y^0, \end{aligned} \tag{10b}$$

$$u_\tau \in U_{ad}^\tau. \tag{10c}$$

Owing to linearity and to finite-dimensionality, the discrete state equation (10b) admits, obviously, for every pair $(y_h^0, u_\tau) \in \mathbf{V}_h \times \mathbf{U}_\tau$ a unique solution $y_{\tau,h}$. This allows us to introduce the analogue of control-to-state operator in discrete case $S_{\tau,h} : U_{ad}^\tau \to L_2(0, T, \mathbf{V}_h) : u_\tau \mapsto y_{\tau,h}$ and to rewrite (10) in condensed form

$$f_\eta^{\tau,h} := J_\eta^{\tau,h}(S_{\tau,h}(u_\tau), u_\tau) \longrightarrow \min_{u_\tau \in U_{ad}^\tau}. \tag{11}$$

The control problem (11) has at least one solution, since U_{ad}^τ is not empty and the problem is penalized. Again, as in the continuous case, the non-convexity of the problem may cause multiple local optima.

2.3. Gradient computation by adjoint techniques

We follow here the 'first discretize, then optimize' strategy. The finite-dimensional problem (10) is a large-scale nonlinear minimization problem with constraints. Using the constraints to eliminate y we arrive at (11) we obtain a large-scale nonlinear minimization problem where the only constraints are the box constraints on the control. Techniques to compute minimizers of such problems involve the evaluation of the gradient of the objective function.

Here, we derive a discrete adjoint equation by applying the standard Lagrangian principle, where the discretized state equation is eliminated by Lagrangian multipliers.

To simplify the notation we use the discrete variables y, u, λ without subscripts τ, h in the following part.

We couple the constraint – M steps of the backward Euler method – by Lagrangian multipliers to $J_\eta^{\tau,h}(y,u)$. The result is abbreviated by J_λ. The Lagrangian multipliers $\lambda^k \in \mathbf{V}_h$ are determined such that the variation of J_λ does not depend on variations of y. This is accomplished by applying the discrete analog of partial integration.

$$\begin{aligned}
7J_\lambda &= J_\eta^{\tau,h}(y,u) + C_\lambda \text{ with} \\
C_\lambda &= \sum_{k=1}^{M} \left(\langle \lambda^k, y^k - y^{k-1} \rangle + \tau a(y^{k-1}; y^k, \lambda^k) - \tau (g(y^{k-1}, u^k), \lambda^k)_\Gamma \right) \\
&= \sum_{k=0}^{M-1} \langle \lambda^k - \lambda^{k+1}, y^k \rangle - \langle \lambda^0, y^0 \rangle + \langle \lambda^M, y^M \rangle \\
&\quad + \tau \sum_{k=1}^{M} \left(a(y^{k-1}; \lambda^k, y^k) - (g(y^{k-1}, u^k), \lambda^k)_\Gamma \right).
\end{aligned}$$

The first variation of $J_\eta^{\tau,h}(y,u)$ is given by

$$\begin{aligned}
\delta J_\eta^{\tau,h}(y,u) = &\sum_{i=1}^{n} \mu_i \langle y_i^M - y_{d,i}, \delta y_i^M \rangle \\
&+ \tau \sum_{k=1}^{M} \int_\Omega P_\eta'(\sigma(y^k)) \, \langle \partial_{y^k} \sigma(y^k), \delta y^k \rangle \, d\Omega + \tau \sum_{k=1}^{M} \sum_{j=1}^{m} \alpha_j (u_j^k - u_{d,j}) \delta u_j^k
\end{aligned}$$

whereas the variation of the coupled constraint evaluates to

$$\begin{aligned}
\delta C_\lambda = &\sum_{k=1}^{M-1} \langle \lambda^k - \lambda^{k+1}, \delta y^k \rangle + \langle \lambda^M, \delta y^M \rangle \\
&+ \tau \sum_{k=1}^{M} a(y^{k-1}; \lambda^k, \delta y^k) + \tau \sum_{k=1}^{M-1} \left\langle \partial_{y^k} a(y^k; \lambda^{k+1}, y^{k+1}), \delta y^k \right\rangle \\
&- \tau \sum_{k=1}^{M-1} \left\langle \partial_{y^k} (g(y^k, u^{k+1}), \lambda^{k+1})_\Gamma, \ \delta y^k \right\rangle - \tau \sum_{k=1}^{M} \partial_{u^k} (g(y^{k-1}, u^k), \lambda^k)_\Gamma \, \delta u^k.
\end{aligned}$$

Putting all together, for the variation of J_λ finally we obtain

$$\delta f_\eta^{\tau,h} = \delta J_\lambda = \tau \sum_{k=1}^{M} \sum_{j=1}^{m} \left(\alpha_j (u_j^k - u_{d,j}) - \partial_{u_j^k} (g(y^k, u^k), \lambda^k)_\Gamma \right) \delta u_j^k$$

whenever λ the terminal condition at $t = t^M$

$$\frac{1}{\tau} \sum_{i=1}^{n} \langle \lambda_i^M + \mu_i (y_i^M - y_{d,i}), v_i \rangle + a(y^{M-1}; \lambda^M, v) = \int_\Omega P'_\eta(\sigma(y^M)) \, \langle \partial_{y^M} \sigma(y^M), v \rangle \, d\Omega$$

$\forall v \in \mathbf{V}_h$ and a discrete recursion

$$\begin{aligned} &\tfrac{1}{\tau} \langle \lambda^k - \lambda^{k+1}, v \rangle + a(y^{k-1}; \lambda^k, v) = - \left\langle \partial_{y^k} a(y^k; \lambda^{k+1}, y^{k+1}), v \right\rangle \\ &+ \left\langle \partial_{y^k} (g(y^k, u^{k+1}), \lambda^{k+1})_\Gamma, v \right\rangle - \int_\Omega P'_\eta(\sigma(y^k)) \, \langle \partial_{y^k} \sigma(y^k), v \rangle \, d\Omega \quad \forall v \in \mathbf{V}_h. \end{aligned}$$

This allows to evaluate the gradient efficiently by a discrete linear parabolic problem.

3. Application to a model for wood drying

As already mentioned, wood drying forms a complex physical model that involves heat and humidity transfer inside the material as well as exchange processes with the surrounding media at the surface of the wood. In the sequel we describe a simplified model which is later used in practical applications of wood drying.

The state variables of our process are moisture content X and temperature ϑ inside the wood specimen, i.e. $y = (X, \vartheta)$. Thereby, X is given by $X = (m_w - m_d)/(m_d)$ where m_w denotes the mass of the wet and m_d the mass of the oven dry material. As control variables $u = (v_L, Y_L, \vartheta_L)$ we have the velocity, absolute humidity and temperature of the surrounding air, respectively. As reference controls $u_d = (v_{L,d}, Y_{L,d}, \vartheta_{L,d})$ we applied $v_{L,d} \equiv 0\,\mathrm{m/s}, Y_{L,d} \equiv 0.01038649\,\mathrm{kg/m^3}, \vartheta_{L,d} \equiv 20^o\mathrm{C}$ ($Y_{L,d}$ corresponds to relative humidity $\varphi_L = 60\%$ and to temperature $\vartheta_L = 20^o\mathrm{C}$). These reference controls serve in fact regularizing terms in the objective function. Their values correspond to typical values from practical experience.

The aim of wood drying is to achieve a given target value X_d of the moisture content X inside the wood specimen. Thus, we have the objective function (1a) with $(y; u) = (X, \vartheta; v_L, Y_L, \vartheta_L)$, $\mu = (1, 0)$ and problem dependent regularization parameters $\alpha = (\alpha_1, \alpha_2, \alpha_3)$.

The stresses σ in (1c), (6) are described in Subsection 3.2. below. The remaining parameters (lower, upper control and stress bounds, target humidity, etc.) will be set in Section 4. on the numerical experiments.

3.1. Heat and mass transfer

Our approach bases upon some heat-and-mass transport model by Vogel [25], where some minor modifications were done.

In the transport model the following simplifying assumptions are made:

1. We ignore the fiber structure, i.e. an isotropic homogeneous hydroscopic material is assumed.
2. For heat and mass transfer through the boundary surface we consider heat conduction and radiation, but condensation by sprayed vapor from outside is not considered.
3. The enthalpy for the phase change of water is restricted to the boundary of the wood specimen.
4. The total moisture distribution is considered as a uniform diffusion process.

Such a minimal model on the one hand is able to explain the main effects of a physical process while on the other hand it limits the computational effort for its solution. The model was justified by experiments for different application cases such as wood drying and humidity diffusion between different climates [20, 2]. This can be seen e.g. in Fig. 1 from [2] which provides a comparison of a fully-coupled simulation based on the code DELPHIN 4 [6] with our minimal model. The maximal differences are $\approx 1\%$.

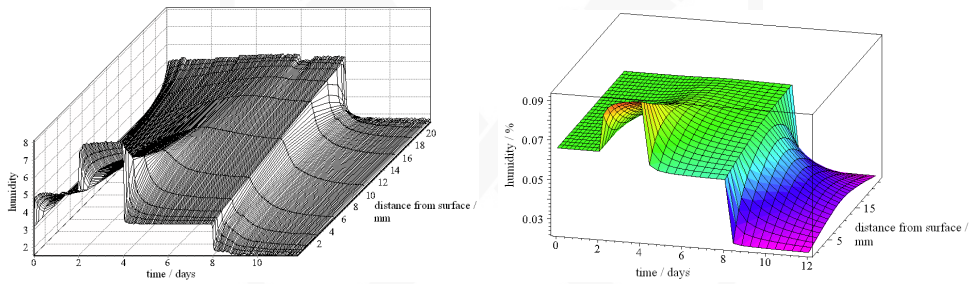

Figure 1.: Comparison of calculation of a diffusion process in wood based materials with the fully-coupled Code DELPHIN 4 (left) and the minimal model (right)

Let $\Omega \subset \mathbb{R}^n$ with $n \in \{2, 3\}$ denote some bounded convex domain with a piecewise smooth boundary $\Gamma = \partial\Omega$ and let $T > 0$ denote some fixed terminal time. The internal stress depends upon the volume changes. These are inflicted by changes of the moisture content field X. Further, the local changes in the moisture content depend upon the temperature field ϑ. Under the made assumptions this can be described by a system of nonlinear parabolic differential equations

$$\begin{aligned} X_t &= \nabla(D(X,\vartheta)\nabla X) && \text{in} \quad \Omega \times (0,T], \\ \vartheta_t &= \frac{1}{\rho_{dt} c_p} \nabla(\lambda(X,\vartheta)\nabla\vartheta) && \text{in} \quad \Omega \times (0,T] \end{aligned} \tag{12}$$

with initial conditions

$$X(\cdot,0) = X^0, \qquad \vartheta(\cdot,0) = \vartheta^0 \quad \text{on} \quad \overline{\Omega}. \tag{13}$$

Here D and λ are the coefficients of diffusion and heat conduction, respectively. These coefficients depend upon the moisture content X and the temperature ϑ. The constant parameters ρ_{dt} and c_p denote the density of the bone-dry wood and the specific heat coefficient, respectively. The heat conduction coefficient $\lambda = \lambda(X,\vartheta)$ is calculated as follows: With some chosen parameter X_{12} (in our calculations $X_{12} = 0.12$) and with with ρ_{dt}, c_p we define

$$\begin{aligned} \rho_{12} &:= \rho_{dt}\,\frac{1+X_{12}}{1+0.84\frac{\rho_{dt}}{1000}X_{12}}, \\ \lambda_0 &:= 0.195\cdot 10^{-3}\rho_{12} + 0.0256, \\ \lambda(X,\vartheta) &:= \lambda_0\,(0.85+1.25X)\left(1-(1.1-0.98\cdot 10^3\rho_{dt})(0.27+\frac{\vartheta}{100})\right). \end{aligned} \tag{14}$$

We model the boundary conditions for the humidity such that the amount of water transported by convection is proportional to the gradient of the inner moisture profile at the boundary. This yields

$$\beta(v_L)(Y_L - Y(X,\vartheta)) = \rho_{dt} D(X,\vartheta)\frac{\partial X}{\partial \nu} \qquad \text{on} \quad \partial\Omega\times(0,T]. \tag{15}$$

For the modeling of vaporization coefficient β the Lewis' analogy

$$\beta(v_L) = \frac{\alpha(v_L)}{c_{pL}}$$

is used, where α denotes the heat-transfer coefficient, v_L is the given velocity of the surrounding air, and $c_{pL} = 1,0054\left[\frac{\text{kJ}}{\text{kgK}}\right]$ the constant air specific heat. Further, Y describes the equilibrium moisture content and depends upon the moisture content X at the surface of the wood as well as upon the temperature ϑ. The control variable Y_L denotes a given moisture profile of the surrounding air.

Now, it remains only to derive the boundary condition for the temperature. The influence of the convective heat flow that controls the drying process is split into its effect upon the material warming and upon the evaporation of water, i.e.

$$\alpha(v_L)(\vartheta_L - \vartheta) = \lambda(X,\vartheta)\frac{\partial\vartheta}{\partial\nu} + \beta(v_L)h_v(X,\vartheta)(Y(X,\vartheta) - Y_L) \ \text{ on } \ \partial\Omega\times(0,T], \tag{16}$$

where α denotes the heat-transfer coefficient, h_v the additively combined bonding and evaporation enthalpy, and ϑ_L the given temperature of the surrounding air. The heat-transfer coefficient due to Krecetov [18] is given by

$$\alpha = \alpha(v_L) = 6.2 + 4.2 v_L,$$

and the enthalpy according to Kayihan–Stanish [16] by

$$h_v(X,\vartheta) = \begin{cases} 267(374-\vartheta)^{0.38}(1+0.4(1-\frac{X}{0.3})), & \text{for } X < 0.3 \\ 267(374-\vartheta)^{0.38}, & \text{otherwise} \end{cases}.$$

For modeling the equilibrium moisture content Y depending on air humidity called sorption hysteresis we apply Krecetov's approach [18]. In this model the moisture X at the boundary of the wood relates to the relative humidity φ and to the temperature ϑ according to

$$X(\varphi,\vartheta)=\begin{cases}\dfrac{0.36}{100}(13.9-B(\vartheta))+\dfrac{0.72}{100}(29.5-B(\vartheta))\,\varphi, & \forall\,\varphi\in[0,0.5]\\ \dfrac{0.512(21.7-B(\vartheta))}{100\,(1.21-\varphi)}, & \forall\,\varphi\in(0.5,1]\end{cases} \tag{17}$$

where $B(\vartheta)=((\vartheta+273.2)/100)^2$. For simplicity we assume that at fiber saturation ($\varphi=1$) independently within the considered temperature range holds $X_{FSP}=0.3$ and that the moisture content X at 50% relative humidity ($\varphi=0.5$) independently of the temperature has the value $X_{1/2}=0.08$. Now, we obtain the required inverse mapping

$$\varphi(X,\vartheta)=\begin{cases}\dfrac{X-\frac{0.36}{100}(13.9-B(\vartheta))}{\frac{0.72}{100}(29.5-B(\vartheta))}, & X\le X_{1/2}\\ 1.21-\dfrac{\frac{0.512}{100}(21.7-B(\vartheta))}{X}, & X_{1/2}<X<X_{FSP}\\ 1.21-\dfrac{\frac{0.512}{100}(21.7-B(\vartheta))}{X_{FSP}}, & X\ge X_{FSP}.\end{cases} \tag{18}$$

The relative humidity φ relates to the absolute humidity Y by

$$Y(X,\vartheta)=\delta\cdot\varphi(X,\vartheta)E(\vartheta), \tag{19}$$

where $\delta=0.622/p$ at the normal pressure $p=1000$[hPa] is a constant and

$$E(\vartheta)=6.1078\cdot\exp\left(\frac{17.08085\cdot\vartheta}{234.175+\vartheta}\right) \tag{20}$$

represents the saturation pressure.

The approach of Dushman–Lafferty [7] for the diffusion coefficient of water vapor D_V below the fiber saturation point yields

$$D_V(X,\vartheta)=0.22\cdot10^{-4}\frac{p}{R}\frac{\rho_w+\rho_{zw}X}{\rho_w\rho_{zw}}\left(\frac{\vartheta+273}{273}\right)^{1.75}\frac{1}{\vartheta}\frac{\partial\varphi}{\partial X}(X,\vartheta), \tag{21}$$

where p is the normal pressure, R the universal gas constant, ρ_w denotes the density of water and ρ_{zw} the density of the cell wall. For ρ_w and ρ_{zw} we put the constant values 1000 [kg/m^3] and 1510 [kg/m^3], respectively. $\dfrac{\partial\varphi}{\partial X}(X,\vartheta)$ in equation (21) means the slope of the absorption isotherms that can be calculated via the formula (18).

The transport of bound water below the fiber saturation point we follows the Arrhenius' law

$$D_B(X,T)=7\cdot10^{-6}\cdot\exp\left(-\frac{E_0(X)}{R(\vartheta+273)}\right),$$

with the universal gas constant R and the activation energy

$$E_0(X) = 3.86 \cdot 10^4 - 2.94 \cdot 10^4 X.$$

Siaus's analogy [21] leads to the following transport model

$$D(X,\vartheta) = \frac{1}{1-a_p(X,\vartheta)^2} \frac{D_B(X,\vartheta) D_V(X,\vartheta)}{D_B(X,\vartheta) + (1-a_p(X,\vartheta)) D_V(X,\vartheta)}, \quad X \le X_{FSP} \quad (22)$$

where a_p denotes the edge length of the cross-section of square pore, that can be calculated from the porosity of the solid body v_a

$$a_p(X,\vartheta) = \sqrt{v_a} \approx \sqrt{1 - \frac{\rho(X)}{\rho_w} \frac{0.667 + X}{1+X}}.$$

The density of the humid wood under the fiber saturation point is given by

$$\rho(X) = \rho_{dt} \frac{1+X}{1 + 0.84X \frac{\rho_{dt}}{1000}}.$$

Above the fiber saturation point, i.e. for $X > X_{FSP}$. we apply Koponen's [17] concept, that uses the diffusion coefficient in fiber saturation point as initial value

$$\begin{aligned} D(X,\vartheta) &= D(X_{FSP},\vartheta)(1 - 0.8845 \cdot k(X) + 0.2525 \cdot k(X)^2) \\ \text{with} \qquad k(X) &= \frac{X - X_{FSP}}{\frac{\rho_w}{\rho_{dt}}(1 - \frac{\rho_{dt}}{\rho_{zw}}) - X_{FSP}}. \end{aligned} \quad (23)$$

The described model can be embedded easily into the abstract mathematical model of the state equation (1b).

3.2. Elastic model for stress evaluation

Our elastic model follows Siimes's [22] model with the simplifying assumptions:

1. The (rectangular) shape of a specimen crosscut remains unchanged during drying.
2. We approximate the total stress by a coordinate splitting approach.
3. The resulting external forces in the x and in the y-direction vanish.

We have to provide a model for the evaluation of the internal stresses σ. The changes in length are denoted by Δl^x and Δl^y and the lengths of specimen in x- and y-direction are defined by l_x and l_y, respectively. The approach is described for the x-direction below, the results for the y-direction are obtained in a similar way.

Moisture content X induces a relative change of the volume as well as a change of the module of elasticity. The volumetric change induces a free strain $\varepsilon^x_{free}(x,y)$. Neglecting shear effects, we have an averaged free length change

$$\Delta l^x_{free}(y) = \int_0^{l_x} \varepsilon^x_{free}(x,y)dx.$$

By Assumption 1, we observe a constant length change

$$\Delta l^x_{obs} = \int_0^{l_x} \varepsilon^x_{obs}(x)dx$$

that is independent of y. The difference of both strains yields the effective strain

$$\varepsilon^x_{eff}(x,y) = \varepsilon_{free}(x,y) - \varepsilon^x_{obs}(x). \tag{24}$$

Now, the stresses follow Hooke's law,

$$\sigma^x(x,y) = E(x,y)\varepsilon^x_{eff}(x,y). \tag{25}$$

Due to Assumption 3 we have

$$\int_0^{l_y} \sigma^x(x,y)\,dy = 0.$$

Hence,

$$\varepsilon^x_{obs}(x) = \frac{\int_0^{l_y} E(x,y)\varepsilon_{free}(x,y)\,dy}{\int_0^{l_y} E(x,y)\,dy}.$$

Combining the stresses in the x- and y-directions, we obtain the total stress

$$\sigma(x,y) = |\sigma^x(x,y)| + |\sigma^y(x,y)|. \tag{26}$$

Finally, we have to supply models for the elasticity module E and the free strain ε_{free}. One possibility is due to Welling [26]

$$E(x,y) = E(X(x,y)) = \begin{cases} E(X=0.08), & X < 0.08 \\ E_B(\rho_{dt})(0.904 - 4.37(X-0.12)), & 0.08 \le X \le 0.18 \\ E(X=0.18), & X > 0.18 \end{cases}$$

where $E_B(\rho_{dt}) = 40 + 2.12 \cdot 10^{-3}\rho^2_{dt}$. Further, we apply the Ansatz

$$\varepsilon_{free}(x,y) = \varepsilon_{free}(X(x,y)) = \begin{cases} \dfrac{\alpha(X=0.3) - \alpha(X)}{1 - \alpha(X=0.3)}, & X < 0.3 \\ 0, & \text{otherwise} \end{cases}$$

with $\alpha(X) = \dfrac{0.84 \cdot 10^{-3}\rho_{dt}X}{1.360 + 4.394 \cdot 10^{-4}\rho_{dt} - 5.179 \cdot 10^{-8}\rho^2_{dt}}$.

4. Numerical experiments

4.1. Simulation of the direct problem

Before we turn to optimal control we have to validate the used simplified model described in the previous sections. For this purpose among other test problems we selected some practical experiment reported in [12]. These results are compared with those obtained by our computer simulation.

The state equations are discretized by piecewise linear C^0-element technique over triangular grids. The underlying finite element geometry was generated by the program package FEMLAB (see http://www.comsol.com/).

As common in wood engineering, we represent the control $u = (v_L, Y_L, \vartheta_L)$, i.e. the air velocity, the absolute air humidity and air temperature in the drying chamber in form of a drying plan. Dry-bulb and wet-bulb temperatures of psychrometer are depicted on the drying plan. The required absolute and relative humidity can be calculated from these data. In our experiments the air velocity was considered as constant.

In addition to the simulated and measured mean humidity, in both examples we describe the moisture development in three reference knots. These knots are chosen in such that they represent typical areas of the specimen. This is achieved by point 1 – at the boundary, point 2 – in the center of the domain and point 3 – inside, but very close to the boundary.

Example 1

In Fig. 4 we illustrate the effect of oscillating relative humidity (compare drying plan, Fig. 3) in form of a stepwise course of the mean humidity of wood. Again, the experimental data are in accordance with the simulation results.

Table 1.: Data for Example 1

Air velocity	$1\frac{\mathrm{m}}{\mathrm{s}}$	Oven dryness	$700\frac{\mathrm{kg}}{\mathrm{m}^3}$
Sample size	38×77 mm	Drying time	250h
Initial humidity	31%	Initial temperature	40°C
Time step size	600s	Spatial step size	3.85 mm

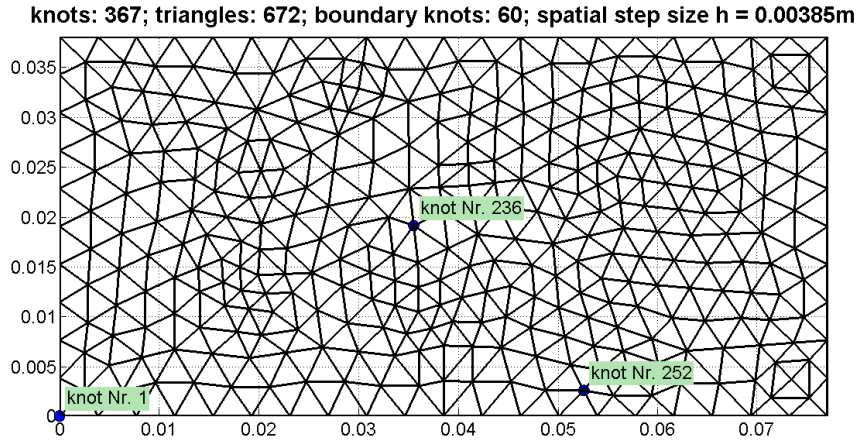

Figure 2.: FEM grid generated by FEMLAB

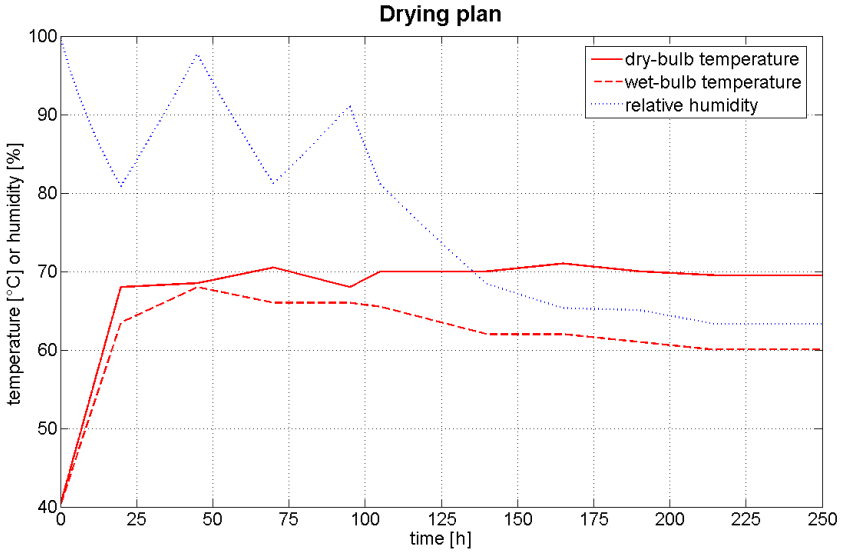

Figure 3.: Given control (drying plan)

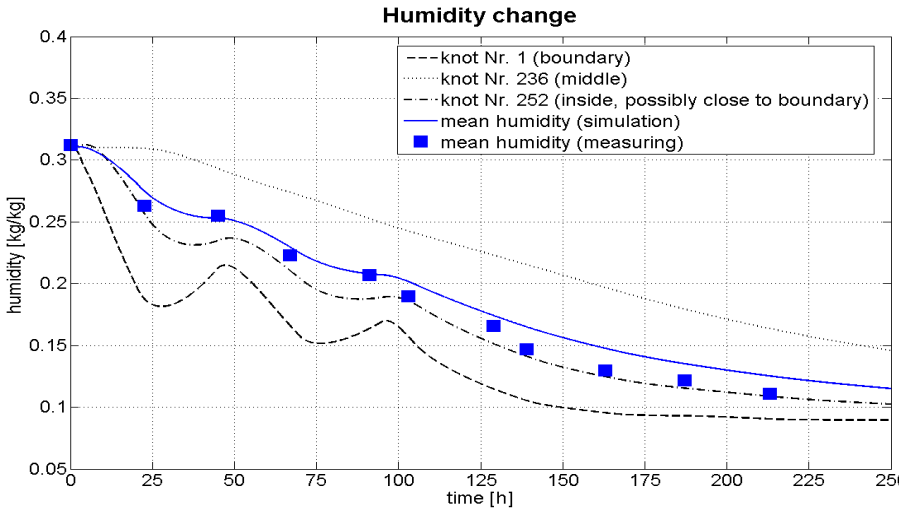

Figure 4.: Humidity change

Table 2.: Deviation of the simulation from the measurement

Error	maximum	mean	root-mean-square
$\left[\frac{\text{kg}}{\text{kg}}\right]$	$0,018$	$0,009$	$0,011$

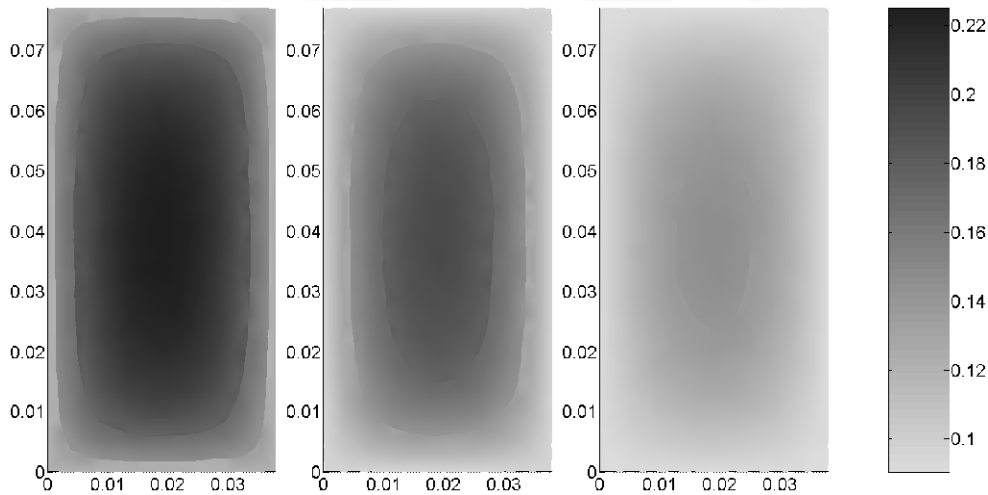

Figure 5.: Humidity distribution after 125h, 167h and 250h

The obtained results for the simulation of the direct problem are qualitatively (see Fig. 4) as well as also quantitatively (compare Tab. 2) in very good agreement with the experimental data. This provides a justification for the use of the simplified presented above for the wanted optimal control.

4.2. Optimal control experiments

While in the previous subsection we reported on some results for the direct problem, i.e. some problem with given controls (drying plans) here we consider the generation of drying plans by optimization techniques. The data of the reported examples are given in the Tab. 3 below. All numerical experiments are executed for the case of zero-regularization (i.e. $\alpha = (\alpha_1, \alpha_2, \alpha_3) = (0, 0, 0)$ in (1a)). This is possible because the penalty already provides a regularizing effect. Furthermore, the control is also penalized, i.e. the term

$$\sum_{i=1}^{3} \int_0^T P_\eta(u_i(t), u_{a,i}, u_{b,i}, s)\, dt$$

is added to the objective function (compare eq. (6)). That leads to an unconstrained optimization problem. As optimization methods gradient based techniques have been applied where the gradients are efficiently evaluated via adjoint equations.

For both examples we have chosen the following triangulation obtained by FEMLAB computer code.

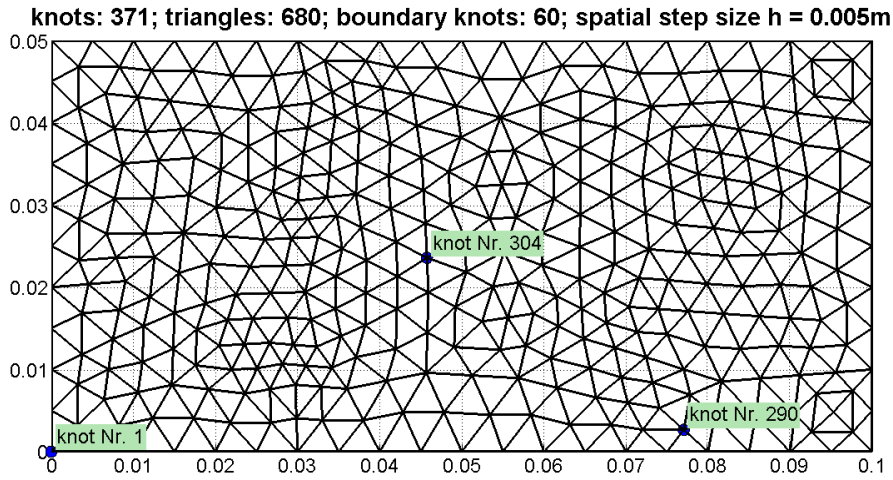

Figure 6.: FEM grid generated by FEMLAB

As already mentioned the table below describes the initial data used in the optimization process. Both examples differ only in the target humidity and in the stress restriction. The initial values for the control are chosen such that the initial humidity and the initial temperature remain constant in time. Due to that fact we can achieve that the initial stress lies in the feasible region.

Table 3.: Initial optimization data

	Example 2	Example 3
Oven dryness	700 kg/m^3	700kg/m^3
Sample size	50×100 mm	50×100 mm
Initial humidity	22%	22%
Initial temperature	8° C	8° C
Time step size	600 s	600 s
Spatial step size	5 mm	5 mm
Drying time	24 h	24 h
Target humidity	**21%**	**16%**
Stress bounds	**±10** mPa	**±25** mPa
Lower control bounds	0 m/s, 5%, 5° C	0 m/s, 5%, 5° C
Upper control bounds	10 m/s, 95%, 85° C	10 m/s, 95%, 85° C

For the optimization a restart version of Broyden's method has been applied with the identity matrix as initial approximation of the Jacobian. After 100 iteration steps the restart procedure, i.e. the iteration matrix is again set to the identity. Further, at restart the penalty parameter is reduced by a fixed multiplier.

Similarly to the direct simulation we choose three reference knots (see Fig. 6) to observe the state of humidity and elastic stress at these points.

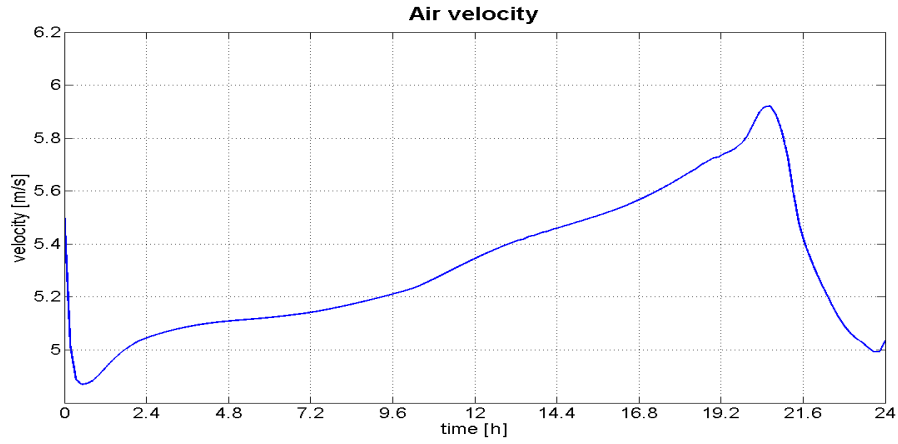

Figure 7.: Computed velocity after 4 iterations Example 2

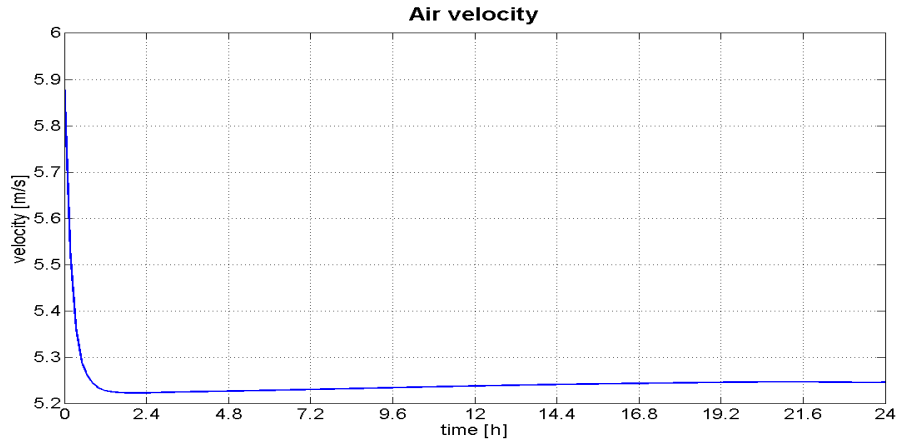

Figure 8.: Computed velocity after 4 iterations Example 3

In case of analyzing the calculated air velocity, one can put the expediency of this parameter as the means of control into question. The hardly relevant velocity variation points out the fact, that the velocity part of the Jacobian $J'(u)$ in comparison to corresponding temperature and moisture parts is negligible small. In both experiments the calculated velocity ranges between 4.8 and 5.9, i.e. rather close to $(v_{L,a} + v_{L,b})/2 = 5\text{m/s}$. This indicates the fact that the velocity is essentially determined by the penalty function $P_\eta(\cdot, v_{L,a}, v_{L,b}; s)$ in case of a rather large smoothing parameter s.

A fluctuating behavior can be observed also in the calculated drying plans for temperature as well as for the humidity. Thus, not only the dehydrating phase, but also the moistening phase can be essential in the drying process, a fact that is applied in practice.

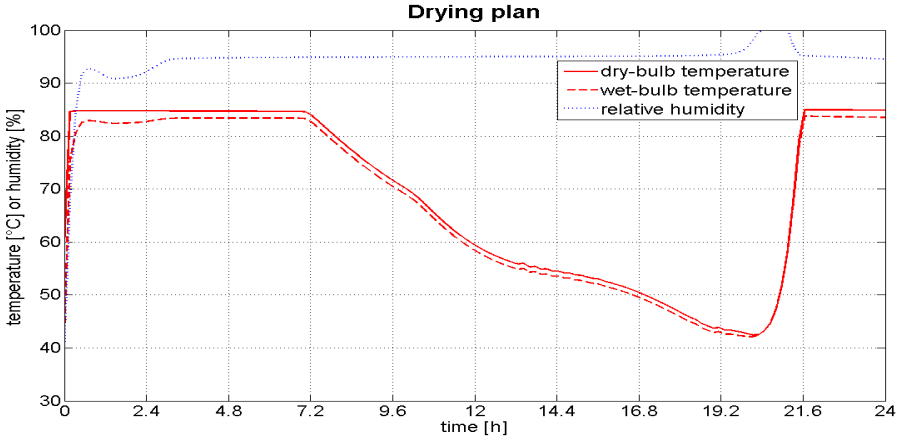

Figure 9.: Obtained control after 4 iterations, Example 2

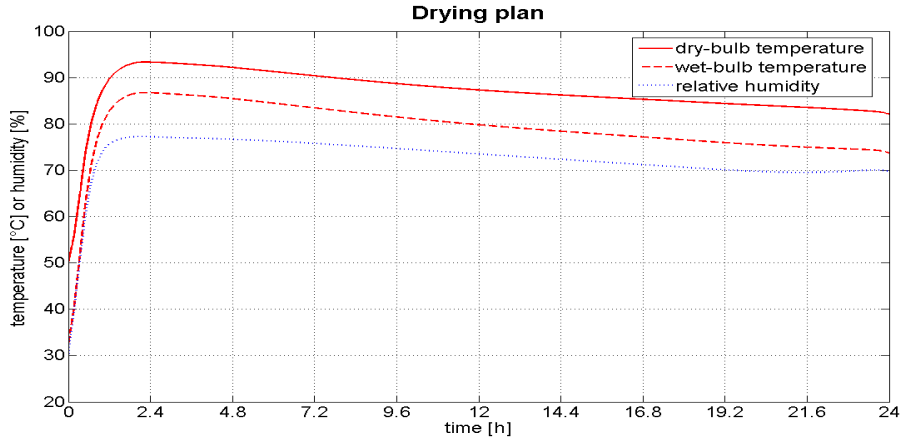

Figure 10.: Obtained control after 4 iterations, Example 3

The qualitative behavior of the optimal control variables differs for the two different experiments. In Example 3 a mean target humidity of 16% (a loss of 6% moisture) after 24 hours is required. Most wood materials even under the relatively weak stress bounds ±25 mPa (see Tab. 3) can lose only a small part of moisture. This leads us to the straightforward solution strategy, in which almost everywhere the highest admissible air temperature and the smallest admissible air humidity are chosen such that the stress bounds are active at the boundary.

In Example 2 a moderate moisture loss of only 1% is required. This leads us to a solution (see Fig. 10, on the left) where the inequality restrictions for the controls are active. The solution has the property that the mean target humidity of 21% is almost achieved. The stress is widely within the given bounds. At the same time (see Fig. 12) the boundary humidity exceeds for a short term the initial humidity (moistening). Interesting is also that the stress at the end of the drying sink is nearly by zero again (see Fig. 14, on the left).

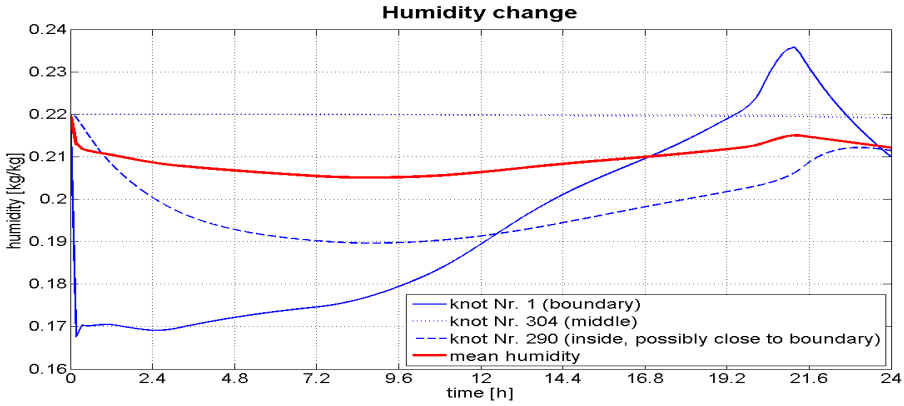

Figure 11.: Humidity in reference knots, Example 2

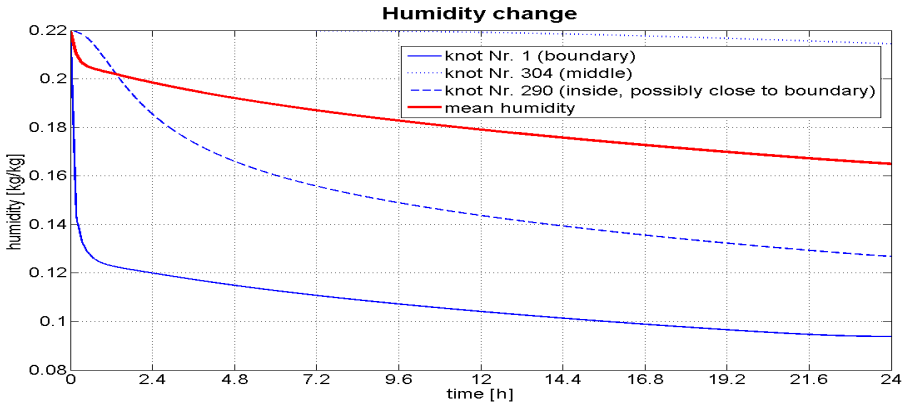

Figure 12.: Humidity in reference knots, Example 3

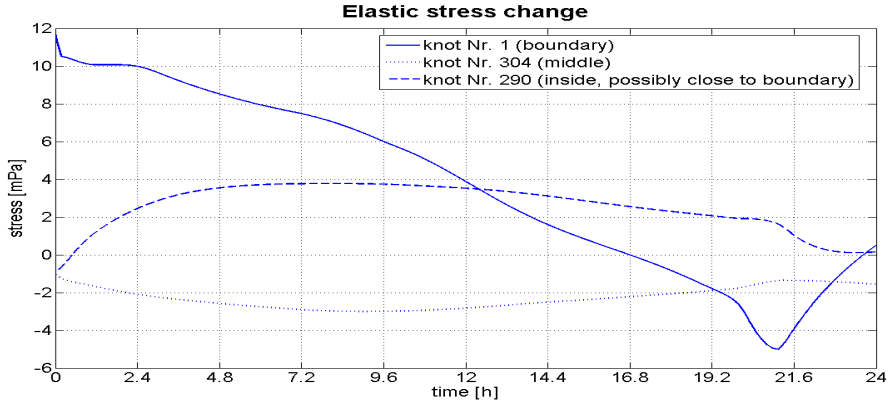

Figure 13.: Stress in reference knots, Example 2

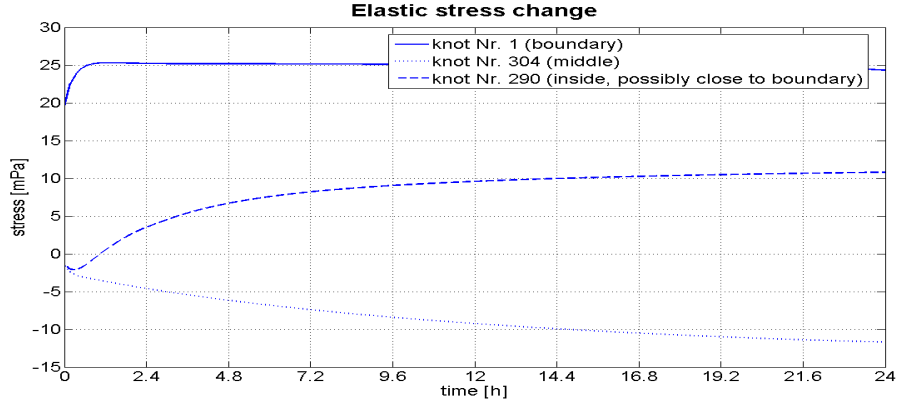

Figure 14.: Stress in reference knots, Example 3

Some quantitative results of both experiments are summarized in Tab. 4. One

can see that the required mean target humidity is almost achieved. The stress and control bounds are both broken.

Table 4.: Some quantitative results

	Example 2	Example 3
Mean humidity (T = 24h)	21.22%	16.49%
Min stress	−5.0 mPa	−11.7 mPa
Max stress	11.9 mPa	25.3 mPa
Min control values	4.8 m/s, 40.0%, 42.4 °C	5.2 m/s, 30.0%, 50.0 °C
Max control values	5.9 m/s, 100.0%, 85.0 °C	5.9 m/s, 77.3%, 93.3 °C

Bounds breaking can be reduced through decreasing of corresponding penalty parameters. The problem of the control bounds breaking can be avoided thanks to application of the methods for the constrained optimization, e.g. [10]. Moreover, if the regularization is used (that means $\alpha \neq 0$, compare Eq. (1a)), it will be automatically provided, that the control lie near the energy minimal control (cost minimization) and so are feasible.

It must be mentioned that the stress bounds in all our experiments are broken only during the short time at the beginning of drying. This result can still be acceptable for the wood drying, since at the beginning, where the moist material has sufficient viscosity, the stress bounds are less critical than during the rest time of drying.

5. References

[1] Amann H.; *Dynamic theory of quasilinear parabolic equations. I. Abstract evolution equations*, Nonlinear Analysis: Theory, Methods and Applications 12, 1988, pp. 895–919.

[2] Branke D., Kröppelin U., Scheffler M., Thielsch K.; *Simulationsmodell fr Holzwerkstoffplatten unter Differenzklimabeanspruchung*, Holztechnologie 48 (1), 2007, pp. 25–29.

[3] Casas E., Mateos M.; *Uniform convergence of the FEM applications to state constrained control problems*, Comput. Appl. Math. 21, 2002, pp. 67–100.

[4] Ciegis R., Starikoviûs V.; *Mathematical modelling of wood drying process*, Math. Model. Anal. 7(2), 2002, pp. 177–190.

[5] Cloutier A., Fortin Y.; *A model of moisture movement in wood based on water potential and the determination of the effective water conductivity*, Wood Sci. Technology 27, 1993, pp. 95–114.

[6] Delphin, TU Dresden, Program system, Institut für Bauklimatik.

[7] Dushman S., Lafferty J.M.; *Scientific foundation of vakuum techique*, Mir, Moskva 1962.

[8] Galant A.; *Mathematische Modelle zur Optimierung von Trocknungsprozessen unter Berücksichtigung von Rissbildungen*, TU Dresden, Graduation thesis, 2007.

[9] Grossmann C., Roos H.-G., Stynes, M.; *Numerical treatment of partial differential equations*, Springer, Berlin 2007.

[10] Grossmann C., Terno J.; *Numerik der Optimierung*, Teubner, Stuttgart 1997.

[11] Grossmann C., Zadlo M.; *A general class of penalty/barrier path-following Newton methods for nonlinear programming*, Optimization 54, 2005, pp. 161–190.

[12] Hardtke H.-J., Militzer K.-E., Fischer R., Hufenbach W.; *Entwicklung und Identifikation eines kontinuumsmechanischen Modells für die numerische Simulation der Trocknung von Schnittholz*, TU Dresden, (Research report DFG-project Ha 2075/3-2), 1997.

[13] Hinze M.; *A variational discretization concept in control constrained optimization: The linear-quadratic case*, Comput. Optim. Appl. 30, 2005, pp. 45–61.

[14] Irudayaraj J., Haghighi K., Stroshine R.L.; *Nonlinear finite element analysis of coupled heat and mass transfer problems with an application to timber drying*, Drying Technology 8, 1990, pp. 731–749.

[15] Kamke F.A., Vanek M.; *Review of wood drying models*, In: Haslett A.N., Laytner F. (eds.); Proc. 4th Int. IUFRO Wood Drying Symposium. August, 1994, Rotorua, NZ For. Res. Inst., Rotorua, New Zealand, pp. 1–21.

[16] Kayihan F., Stanish M.A.; *Wood particle drying, a mathematical model with experimental evaluation*, In: Mujumdar A.S. (ed.); Drying '84. Hemisphere publ. corp. New York 1984, pp. 330–347.

[17] Koponen H.; *Moisture diffusion coefficients of wood*, In: Mujumdar A.S.; Drying '87. Hemisphere publ. corp. New York 1987, pp. 225–232.

[18] Krečetov U.V.; *Suška drevesiny*, Lesnaja promyšlennost, Moskva 1972.

[19] Luikov A.V.; *Heat and mass transfer in capillary-porous bodies*, Pergamon Press, London 1966.

[20] Scheffler M.; *Bruchmechanische Untersuchungen zur Trockenrissbildung an Laubholz*, TU Dresden, Dissertation thesis, 2000.

[21] Siau J.F.; *Transport processes in wood*, Springer, Berlin 1984.

[22] Siimes F.; *The effect of specific: gravity, moisture, temperature and heating time on the tension and compression strength and elasticity properties perpendicular to the grain of finnish pine spruce and birch wood and the significance of these factors on the checking of timbers at kiln drying*, State Inst. Technical Res., Finland, Publ. 84, Helsinki 1967.

[23] Thomas H.R., Lewis, R.W., Morgan, K.; *An application of the finite element method to the drying of timber*, Wood Fibre 11, 1980, pp. 237–243.

[24] Tröltzsch F.; *Optimal Control of Partial Differential Equations. Theory, Methods and Applications*, Amer. Math. Soc. (AMS), Providence, RI, 2010.

[25] Vogel R.; *Modellierung des Wärme- und Stofftransportes und des mechanischen Spannungsfeldes bei der Trocknung fester Körper am Beispiel der Schnittholztrocknung*, TU Dresden, Dissertation thesis, 1989.

[26] Welling J.; *Die Erfassung von Trocknungsspannungen während der Kammertrocknung von Schnittholz*, Hamburg, Dissertation thesis, 1987.

[27] Zeidler E., Nonlinear Functional Analysis and its Applications. II/B: Nonlinear Monotone Operators, Springer Verlag, New York 1990.